Removal of developmentally regulated microexons has a minimal impact on larval zebrafish brain morphology and function

Caleb C.S. Calhoun[1], Mary E.S. Capps[1,2], Kristie Muya[1], William C. Gannaway[1], Verdion Martina[1], Claire L. Conklin[1], Morgan C. Klein[1], Jhodi M. Webster[1], Emma G. Torija-Olson[1], Summer B. Thyme[1,2]*

1. Department of Neurobiology, The University of Alabama at Birmingham Heersink School of Medicine, Birmingham, AL, USA
2. Present Address: Department of Biochemistry and Molecular Biotechnology, UMass Chan Medical School, Worcester, MA, USA

* Correspondence may be addressed to Summer B. Thyme (Email: Summer.Thyme@umassmed.edu).

Abstract

Microexon splicing is a vertebrate-conserved process through which small, often in-frame, exons are differentially included during brain development and across neuron types. Although the protein sequences encoded by these exons are highly conserved and can mediate interactions, the neurobiological functions of only a small number have been characterized. To establish a more generalized understanding of their roles in brain development, we used CRISPR/Cas9 to remove 45 microexons in zebrafish and assessed larval brain activity, morphology, and behavior. Most mutants had minimal or no phenotypes at this developmental stage. Among previously studied microexons, we uncovered baseline and stimulus-driven phenotypes for two microexons (meA and meB) in *ptprd* and reduced activity in the telencephalon in the *tenm3* B_0 isoform. Although mild neural phenotypes were discovered for several microexons that have not been previously characterized, including in *ppp6r3*, *sptan1*, *dop1a*, *rapgef2*, *dctn4*, *vti1a*, and *meaf6*. This study establishes a general approach for investigating conserved alternative splicing events and prioritizes microexons for downstream analysis.

Introduction

Alternative splicing greatly expands proteome diversity and can impact brain development and disease (Vuong et al., 2016). As most metazoan proteins are represented by multiple isoforms, defining the functional significance of individual splicing events is a vast challenge. Mouse studies do not have the throughput to assess the neural role of 10s or 100s of isoforms, and cell culture does not recapitulate the complex development of an animal brain.

One class of particularly conserved and developmentally regulated spliced exons is microexons or mini-exons. These small exons, defined here as 3-30 nucleotides or 1-10 amino acids in length, are either gained or lost in transcripts in the brain compared to other tissues. While most are in-frame, this pathway can also trigger nonsense-mediated decay to influence protein levels (Lin et al., 2020). Although these neuron-specific exons were recognized almost 40 years ago (Brugge et al., 1985; Martinez et al., 1987), their discovery and annotation have continued into recent years (Parada et al., 2021). Thus far, hundreds have been identified. Although more than

one splicing regulator has been implicated in the alternative inclusion of microexons in neurons (Ciampi et al., 2022; Y. I. Li et al., 2015), many are controlled by the vertebrate-specific protein SRRM4 (Irimia et al., 2014; Quesnel□Vallières et al., 2015). Srrm4 interacts with Srsf11 and Rnps1 at polypyrimidine sequences upstream of microexons to regulate their inclusion (Gonatopoulos□Pournatzis et al., 2018).

Proteins that regulate and contain microexons are involved in neurodevelopmental disorders. In the brains of individuals with autism spectrum disorder (ASD), the level of SRRM4 is reduced, leading to the misregulated splicing of multiple microexons (Irimia et al., 2014). Mice haploinsufficient for Srrm4 display reduced social interaction, sensory hypersensitivity, and impaired synaptic transmission (Quesnel□Vallières et al., 2015). Furthermore, Srrm4 is involved in regulating the ASD-relevant KCC2-dependent GABAergic excitatory to inhibitory switch (Nakano et al., 2019), and a mouse model of ASD with disrupted *Pten* has decreased Srrm4 expression and microexon inclusion (Thacker et al., 2020). Loss-of-function variants in its interacting partner SRSF11 have been implicated in ASD in humans (C Yuen et al., 2017). While the behavioral roles of only a few microexons have been studied in detail (Gonatopoulos□Pournatzis and Blencowe, 2020), the elimination of one from Eif4g1 altered synaptic plasticity and social behavior in mice (Gonatopoulos□Pournatzis et al., 2020). Many genes containing microexons also lead to neurodevelopmental disorders when mutated in humans. Examples include *CASK*-mediated microcephaly and cerebellar hypoplasia, *SPTAN1*-mediated childhood-onset epilepsy, and *MAPK8IP3*-mediated intellectual disability (Giacomini et al., 2021; Platzer et al., 2019; Syrbe et al., 2017). Taken together, this splicing program, the genes with microexons, and microexons themselves are important to enable proper neural development.

Although most microexons are unstudied, detailed structural and functional characterization of a small subset has revealed involvement in synapse development. The most well-studied are found in the receptor-type tyrosine phosphatase (e.g., *ptprf*) and teneurin (e.g., *tenm4*) gene families. Recognized in the 1990s (O'Grady et al., 1994; Pulido et al., 1995), two microexons in presynaptic PTPδ (*Ptprd*), PTPσ (*Ptprs*), and LAR (*Ptprf*) modulate *trans*-synaptic interfaces and determine selective interaction with postsynaptic partners (Lin et al., 2018; Y. Li et al., 2015; Park et al., 2020; Um et al., 2014; Yamagata et al., 2015; Yim et al., 2013). Similarly, differential inclusion of two conserved microexons in teneurins can modulate *trans*-synaptic homophilic or heterophilic interactions through splicing-dependent, large conformational changes (Berns et al., 2018; Gogou et al., 2024; Li et al., 2020). While studying these cell adhesion molecules has highlighted how microexons can trigger differential protein-protein interactions, little is known about the developmental consequences of these biochemical switches in other protein classes.

Identifying the neurobiological roles of many individual microexons is a challenge. Studies of splicing regulators such as *srrm4* impact the entire splicing program, making it impossible to determine the importance of individual microexons to protein function. Furthermore, microexons could still be differentially included in a *srrm4* regulatory mutant via compensation by other splicing factors, such as its paralogue *srrm3*, which is responsible for microexon inclusion in photoreceptor transcripts in zebrafish (Ciampi et al., 2022). A vertebrate model is necessary for these studies; although there is a similar splicing mechanism in *Drosophila melanogaster*, there

is no overlap of the individual microexons (Torres-Mendez et al., 2021). Thus, we used larval zebrafish, a vertebrate that supports more high-throughput studies than mammalian models (Thyme et al., 2019), to assess the brain activity, brain structure, and behavior of zebrafish larvae mutant for 45 microexons (**Figure 1A**).

Results

A recently developed computational tool identified microexons that are differentially spliced during mouse brain development and conserved in zebrafish (Parada et al., 2021). Based on the intersection of these two sets, 95 microexons fulfilled both parameters (**Table S1**). Of these 95 microexons, 42 exist in a canonical layout in the zebrafish genome, with both a UGC and UC repeat – or similar polypyrimidine tract – directly upstream of the alternatively spliced exon (Gonatopoulos-Pournatzis et al., 2018) (**Table S1**, **Figure S1**), indicating that Srrm4 likely controls their inclusion. Of the remaining microexons, 44 are organized similarly to the canonical layout, typically with either a UGC or UC repeat. Thus, they may also be regulated by Srrm4. The protein sequences of the 95 microexons are highly conserved between mouse and zebrafish (**Figure 1B**), more so than the full-length protein sequences (**Figure 1C**). The genes containing microexons are enriched for those involved in neuronal development as well as the cytoskeleton (**Figure 1D**). The majority of these microexons are included in transcripts as the brain develops, rather than lost, in both mouse and zebrafish (**Figure 1E**), making CRISPR/Cas9 removal of the microexon an ideal approach for studying the function of the added amino acids.

Using CRISPR/Cas9, we generated lines that removed 45 conserved microexons (**Table S2**) and assayed larval brain activity, brain structure, and behavior (**Figure 1A**). Four guide RNAs were used, two on each side of the microexon (**Table S2**, **Figure S1**). For microexons with upstream regulatory elements that are likely important for splicing, these elements were also removed (**Figure S1**). While we were most interested in those microexons only present after 24 hours post-fertilization (**Figure 1E**), as this is when the brain is forming, we also removed microexons from several genes with an earlier expression of the isoform. For eight mutant lines, we confirmed that the microexon was eliminated from the transcripts as expected (**Figure S2**). Although our genomic deletion did not yield unexpected isoforms, qRT-PCR on these eight lines revealed significant downregulation for the homozygous *vav2* mutant (**Figure S2**), indicating possibly complex genetic regulation. Protein-truncating mutations in eleven additional genes that contain microexons revealed developmental and neural phenotypes in zebrafish (**Figure S3**, **Figure S4**), indicating that the genes themselves are involved in biologically relevant pathways. Three of these genes – *tenm4*, *sptan1*, and *ppp6r3* – are also in our microexon line collection.

To uncover neural phenotypes, we assessed baseline and stimulus-driven movement. Homozygous mutant and control sibling larvae were subjected to a behavioral pipeline in 96-well plates from 4-7 days post-fertilization (dpf) (**Figure 2A**). Only a small number of strong, repeatable phenotypes were observed either at baseline or in response to acoustic or visual stimuli (**Figure 2B**, **Figure 2C**, **Figure S5**, **Figure S6**, **Figure S7**). Baseline behavioral differences were observed in multiple movement categories. For example, *rapgef2* mutants showed an increased movement frequency (**Figure 2B**, **Figure 2D**) but no changes to the characteristics of these movements (magnitude) or location in the well. In contrast, *dop1a* mutants had reduced daytime movement and an increased well-edge preference specifically at

night (**Figure S6**, **Figure S8**, **Figure 2B**, **Figure 2D**). Other baseline movement phenotypes included a well-center preference for *vav2* mutants, a decreased movement magnitude for *ptprd*-2 (also referred to in the literature as meA) mutants (**Figure S8**), and an increased movement magnitude for *ptprd*-1 (also referred to in the literature as meB) mutants (**Figure 2D**). Dark-flash response phenotypes included a reduced latency for *eif4g3b* mutants and a reduced response frequency for *ptprd*-1 (meB) and *dop1a* mutants (**Figure 2C**, **Figure 2D**, **Figure S8**). Acoustic response phenotypes included an increased frequency of response to strong stimuli for *ppp6r3* mutants and a reduced frequency of response to strong acoustic stimuli for *ptprd*-2.

To detect changes to brain development and function, we collected phospho-Erk (pErk) brain activity maps under unstimulated conditions at 6 dpf. Large morphological differences were identified using the Jacobian matrix derived from the image registration process (Jefferis et al., 2007; Rohlfing and Maurer, 2003). Similar to the behavioral findings, few phenotypes were observed in brain activity (**Figure 3A**, **Figure S9**, **Figure S10**) or brain structure (**Figure 3B**, **Figure S11**, **Figure S12**) in homozygous mutants compared to wild-type control siblings when quantified by region (**Figure 3C**). Repeatable phenotypes were mild (**Figure 3D**) compared to a mutant with a moderate phenotype and both increased and decreased activity and structure (see control-*tcf7l2*) (Capps et al., 2024). Only one mutant, *ppp6r3*, displayed substantial and repeatable differences in brain morphology (**Figure 3B**, **Figure 3E**), with reduced size observed mainly in the thalamus and neighboring pretectum. While the loss of both copies of microexons was required for most phenotypes, brain activity differences were observed in *vti1a* and *sptan1* heterozygotes (**Figure 3F**) as well as *vav2* and *mapk8ip3* (**Figure S9**, **Figure S10**). While repeatable phenotypes in brain activity and structure were observed in a small subset of mutants, other zebrafish studies using identical methods have typically uncovered brain activity phenotypes for approximately half of the lines that are stronger than any we observed (**Figure 3G**) (Capps et al., 2024; Thyme et al., 2019; Weinschutz Mendes et al., 2023).

Discussion

Our study provides a broad overview of the larval zebrafish neural phenotypes resulting from removing developmentally regulated microexons. Here, we leveraged our previously successful brain activity mapping and behavioral profiling strategy, which has high sensitivity and has uncovered phenotypes for dozens of mutants (Thyme et al., 2019). While only a few zebrafish lines had neural phenotypes, most of the microexons with behavioral or brain activity differences were previously unstudied and found in diverse protein classes.

The small number of observed phenotypes was unexpected based on conservation of the microexons (**Figure 1B**, **Figure 1C**) and the discovery rates of previous screens using similar methods (Capps et al., 2024; Thyme et al., 2019; Weinschutz Mendes et al., 2023). Although most of these studies focused on protein-truncating alleles, we have found phenotypes in lines with missense mutations (Capps et al., 2024). However, this outcome is consistent with a recent, similar study of microexons in zebrafish (Lopez□Blanch et al., 2024). Although only three of the 18 microexons this group studied are in the same genes as our set (*ap1g1*, *vav2*, and *vti1a*), the phenotypes for individual mutants are similar and this work shares the same overall finding of minimal phenotypes in zebrafish larvae. Importantly, the pErk brain activity mapping method we used is highly sensitive, significantly minimizing the likelihood that substantial zebrafish larval

phenotypes from individual microexon removal are being missed. In our published work (Capps et al., 2024; Thyme et al., 2019), we showed that brain activity can be drastically impacted without manifesting in differences in those behaviors assessed in a typical larval screen such as was completed by Lopez-Blanch et al.. Furthermore, the genes that contain microexons are developmentally important (**Figure S3**, **Figure S4**). For instance, the *caska* loss-of-function mutant displayed substantial changes to brain activity, a smaller brain size, and multiple behavioral phenotypes. Loss-of-function mutants for *sptan1* and *ppp6r3* are stronger than lines that only remove the microexon (**Figure S3**, **Figure S4**).

The limited effects of individual microexon deletions suggest that stronger phenotypes may require disrupting multiple microexons or examining later stages of development. It is possible that perturbation of multiple microexons simultaneously, as was observed in the brains of autistic individuals (Irimia et al., 2014), is necessary to produce pronounced effects on early neurodevelopment. Zebrafish homozygous for *srrm4* deletion did not display any overt developmental phenotypes (Ciampi et al., 2022), in contrast to a previous morpholino study (Calarco et al., 2009). More recently, it was revealed that loss of *srrm4* has minimal impacts on behavior (Lopez□Blanch et al., 2024) and brain structure (Gupta et al., 2025), while *srrm3* mutants have significant neural phenotypes and early mortality (Ciampi et al., 2022; Lopez□Blanch et al., 2024). This finding indicates that Srrm3 loss is necessary for complete elimination of these microexons, but studying microexons in the context of this line is also complicated by possible downstream consequences of severe vision loss. Alternatively, although the microexons are present at larval stages, they may only become important during later stages of neuronal maturation that support more complex behaviors. Mouse models were studied as adults and for disruptions to social interaction, learning, and memory (Gonatopoulos□Pournatzis et al., 2020; Han et al., 2024), which larvae are not yet capable of (Dreosti et al., 2015; Valente et al., 2012).

Our study extends on findings for previously studied genes containing microexons. We discovered increased brain activity (**Figure 3D**) and an altered dark flash response in mutants for the *eif4g3b* (**Figure 2D**), whereas a mouse model with the microexon removed was described as having no behavior phenotypes (Gonatopoulos□Pournatzis et al., 2020). That study, however, focused on social behavior, learning, and memory and may not have included stimuli analogous to dark flashes. Alternatively, microexon removal in zebrafish could have differential behavioral impacts than in rodents. Mice mutant for the *ptprd*-2 (meA) microexon have increased movement and interrupted sleep (Park et al., 2020). Both zebrafish mutants in *ptprd* demonstrate the opposite, with reduced daytime movement and increased sleep during the day for *ptprd*-2 (**Figure S8**). While the underlying disrupted circuitry could differ between the species, the daytime sleep increase raises the possibility of a rebound response to undetected nighttime sleep disruptions. In other cases, the gene that contains the microexon has been extensively studied, but research on the microexon itself is absent. For example, the function of SNARE protein Vti1a in neural development and dense core vesicle biogenesis has been studied in great depth (Bollmann et al., 2022; Emperador□Melero et al., 2018; Kunwar et al., 2011; Sokpor et al., 2021; Walter et al., 2014). Its brain-specific microexon, however, was recognized over twenty years ago (Antonin et al., 2000), and its specific importance has been largely ignored. We discovered reduced brain activity mainly in the telencephalon in both homozygous and

heterozygous lines compared to wild-type siblings (**Figure 3F**), highlighting the relevance of considering multiple conserved isoforms when characterizing protein function in the brain.

Mutants for unstudied microexons with the strongest phenotypes come from diverse protein classes (Gonatopoulos Pournatzis and Blencowe, 2020), indicating this splicing program impacts neurodevelopmental processes beyond *trans*-synaptic partner selection. The only mutant with a substantial brain size difference was *ppp6r3*, which encodes a regulator of protein phosphatase 6 (PP6), and this reduced size was present and more severe in the predicted protein-truncating *ppp6r3*^{sa16892} line (**Figure S3**). Although little is known about this protein, it has been linked to cell cycle (Heo et al., 2020) and cell death (Wu et al., 2022), nominating hypotheses for determining future research on the source of the reduced size. Dctn4 is part of the dynactin complex, Mapk8ip3 is involved in Kinesin-1-Dependent axonal trafficking (Platzer et al., 2019; Watt et al., 2015), and Sptan1 is a cytoskeleton scaffold protein (Huang et al., 2017); the number microexon-containing genes related to the cytoskeleton (**Figure 1D**) and also trafficking (e.g., *vti1a*), suggests that microexons may be important to the specialized cytoskeletal needs of developing neurons. The functions of microexons in cytoskeletal proteins are beginning to be discovered (Poliński et al., 2023). Transcriptional regulation is represented by the *meaf6* mutant, while Rapgef2, which has the strongest behavioral phenotypes upon microexon removal (**Figure 3D**), is a signaling protein.

Although our list is not comprehensive, as many microexons remain unstudied, we have prioritized several microexons for future study from the 45 tested. For seven mutants, we confirmed that the microexon was cleanly removed without unanticipated effects on isoforms or transcript levels (**Figure S2**), including for some of the most interesting that are entirely unstudied (*ppp6r3*, *sptan1*, *meaf6*). For those with phenotypes that are not yet confirmed by qRT-PCR (*rapgef2*, *dctn4*, *dop1a*, *mapk8ip3*), studies of gene loss-of-function in zebrafish and mice reveal far stronger phenotypes and lethality, suggesting that our lines impact only the microexon (Abeler Dörner et al., 2020; Drerup and Nechiporuk, 2013; Satyanarayana et al., 2010; Tuttle et al., 2019). In future work, proximity-dependent ligation in zebrafish lines with and without the microexon could reveal differential binding partners *in vivo* (Rosenthal et al., 2021), as microexons are often found in surface-accessible protein domains and can regulate protein-protein interactions (Dergai et al., 2010; Irimia et al., 2014), The discovery of microexon mutants with neural phenotypes lays the groundwork for future investigation of impacted neurodevelopmental pathways and how interactomes differ between isoforms.

Materials and Methods

<u>Zebrafish husbandry</u>

Zebrafish experiments were approved by the UAB Institutional Animal Care and Use Committee (IACUC protocols 22155 and 21744) and UMass Chan Institutional Animal Care and Use Committee (IACUC protocol 202300000053). Mutants were generated in an Ekkwill-based strain using CRISPR/Cas9 as previously described (Capps et al., 2024; Thyme et al., 2019) (Table S2). Both adults and larvae were maintained on a 14 h/10 h light/dark cycle at 28°C. Experimental larvae were maintained at a density of less than 160 per dish in 150 mm petri dishes in fish water with methylene blue, and debris was removed at least twice prior to experimentation. Visibly unhealthy larvae and those without inflated swim bladders were

excluded from experiments. Control animals were always siblings from the same clutch and derived from a single parental pair, and all larvae were genotyped after experimentation. Even with using sibling controls and collecting multiple biological replicates from individual parents, the possibility remains that linked genetic variation may have contributed to the mild phenotypes we observed, as only a single line was generated.

Brain activity and morphology

Phosphorylated-ERK (pErk) antibody staining was conducted as previously described (Capps et al., 2024; Thyme et al., 2019). The total ERK antibody (Cell Signaling, #4696) was used at 3:1000 and pErk antibody was used at 1:500 (Cell Signaling, #4370). Typically, the primary antibody exposure was for 2-3 days and secondary for one day. Image stacks were collected with a Zeiss LSM 900 upright confocal microscope using a 20x/1.0 NA water-dipping objective. These stacks were registered to the standard zebrafish Z-Brain reference using Computational Morphometry Toolkit (CMTK) (Jefferis et al., 2007; Randlett et al., 2015; Rohlfing and Maurer, 2003; Thyme et al., 2019). The significance threshold for MapMAPPING (Randlett et al., 2015; Thyme et al., 2019) was set based on a false discovery rate (FDR) where 0.05% of control pixels would be called as significant for both the brain activity and structural measurements.

Larval behavior

Larval behavior assays were conducted and analyzed as previously described (Capps et al., 2024; Joo et al., 2020; Thyme et al., 2019). The pipeline begins on the evening of larval stage 4 dpf and includes the following stimuli: 5 dpf light flashes (9:11-9:25), mixed acoustic stimuli (prepulse, strong, and weak, from 9:38-2:59), and three blocks of acoustic habituation (3:35-6:35); the night between 5 and 6 dpf mixed acoustic stimuli (1:02-5:00) and light flashes (6:01-6:20); 6 dpf three blocks of dark flashes with an hour between them (10:00-3:00) and mixed acoustic stimuli and light flashes (4:02-6:00). Stimulus responses were quantified from high-speed (285 frames-per-second) 1-second-long movies. All code for behavior analysis is available at https://github.com/thymelab/ZebrafishBehavior. Frequency of movement, magnitude of movement, and location preferences were calculated for the baseline data. An example of a “frequency” measure would be the active seconds / hour. An example of the “magnitude” measure would be the movement velocity of a bout. An example of a “location” measure would be the fraction of the bout time spent in the center of the well. Frequency, response magnitude parameters, and latency to response are also calculated for each stimulus response from the high-speed movies. The stimulus responses are also broken up into subsets, such as the dark flashes that occur at the beginning of the dark flash block and those that occur at the end. Multiple measures are calculated for the experiment, and both summarized and raw measures are shown in Figure 2 and the Supplementary Material. The summarized data is generated by merging related terms (e.g., all the “frequency” measures) together. The size of the bubble represents the percent of significant measurements in the summarized category, and the color represents the mean of the strictly standardized mean difference (SSMD) of the significant assays in that category. It is possible for some measures in the merged group to be increased (purple) and some decreased (orange), such as if a behavioral change occurs between 4 and 6 dpf, which is why it is possible to have two offset bubbles in each square. The scripts for merging these measurements and generating the summarized bubble plot graphs are available at https://github.com/thymelab/DownstreamAnalysis.

Reverse Transcription PCR (RT-PCR and qRT-PCR)

RNA was extracted from zebrafish embryos using the E.Z.N.A. MicroElute Total RNA Kit (Omega Bio-Tek R6834-02), and cDNA synthesis was performed with iScript Reverse Transcription Supermix (Bio-Rad #1708840). Following PCR with GoTaq polymerase (Promega M7123) and primers (Table S1), samples were run on a 4% agarose gel and the band intensities were quantified using Fiji (Schindelin et al., 2012). For qRT-PCR, we combined 3-4 zebrafish heads at 6 dpf for each biological replicate. For RT-PCR, these separate biological samples were combined into one per genotype. We homogenized the heads and performed RNA extraction and cDNA synthesis as described above. We then performed qRT-PCR with SsoAdvanced Universal SYBR Green Supermix (Bio-Rad #1725270EDU) according to the manufacturer's protocol and using primers in Table S1.

Data and materials availability

The mutants described in the paper are available from ZIRC. Code is available from https://github.com/thymelab. Processed behavioral and imaging data is available from Zenodo under the following DOIs: 10.5281/zenodo.13137486 (behavior output files), 10.5281/zenodo.13138646 (behavior input files), and 10.5281/zenodo.13138766 (brain activity mapping stacks).

Acknowledgments

This research was supported by a Mallinckrodt Award from the Edward Mallinckrodt Jr. Foundation (SBT). Guillermo Parada was instrumental to this work by sharing his list of conserved and developmentally regulated microexons while his study was still a preprint under review. We thank the UAB fish facility staff, UMass Chan fish facility staff, the Zebrafish International Resource Center (ZIRC), particularly Andrzej Nasiadka, the Research Computing team at UAB, and the UAB Department of Neurobiology for supporting this study. We also thank the following Thyme lab members for experimental assistance or training that supported this study: Brandon Bastein, Anna Moyer, Lynne Zhou, Vaishnavi Balaji, Alexia Barcus, and Sahil Malhotra.

Author contributions

SBT conceived of the study, analyzed imaging and behavioral data, and wrote the manuscript. VM, JW, and CLC generated the mutant lines. CCSC and KM initiated the project and CCSC collected most of the experimental data. MESC, WCG, MCK, CLC, and EGT contributed to the experimental data in this work by genotyping and propagating zebrafish lines, running larval behavior experiments, and collecting brain imaging data.

References

Abeler-Dörner L, Laing AG, Lorenc A, Ushakov DS, Clare S, Speak AO, Duque-Correa MA, White JK, Ramirez-Solis R, Saran N, Bull KR, Morón B, Iwasaki J, Barton PR, Caetano S, Hng KI, Cambridge E, Forman S, Crockford TL, Griffiths M, Kane L, Harcourt K, Brandt C, Notley G, Babalola KO, Warren J, Mason JC, Meeniga A, Karp NA, Melvin D, Cawthorne E, Weinrick B, Rahim A, Drissler S, Meskas J, Yue A, Lux M, Song-Zhao GX, Chan A, Ballesteros Reviriego C, Abeler J, Wilson H, Przemska-Kosicka A, Edmans M, Strevens N, Pasztorek M, Meehan TF, Powrie F, Brinkman R, Dougan G, Jacobs W, Lloyd CM, Cornall RJ, Maloy KJ, Grencis RK, Griffiths GM, Adams DJ, Hayday AC. 2020. High-throughput phenotyping reveals expansive genetic and structural underpinnings of immune variation. *Nat Immunol* **21**:86–100. doi:10.1038/s41590-019-0549-0

Antonin W, Riedel D, von Mollard GF. 2000. The SNARE Vti1a-beta is localized to small synaptic vesicles and participates in a novel SNARE complex. *J Neurosci* **20**:5724–5732. doi:10.1523/JNEUROSCI.20-15-05724.2000

Berns DS, DeNardo LA, Pederick DT, Luo L. 2018. Teneurin-3 controls topographic circuit assembly in the hippocampus. *Nature* **554**:328–333. doi:10.1038/nature25463

Bollmann C, Schöning S, Kotschnew K, Grosse J, Heitzig N, Fischer von Mollard G. 2022. Primary neurons lacking the SNAREs vti1a and vti1b show altered neuronal development. *Neural Dev* **17**:12. doi:10.1186/s13064-022-00168-2

Brugge JS, Cotton PC, Queral AE, Barrett JN, Nonner D, Keane RW. 1985. Neurones express high levels of a structurally modified, activated form of pp60c-src. *Nature* **316**:554–557. doi:10.1038/316554a0

C Yuen RK, Merico D, Bookman M, L Howe J, Thiruvahindrapuram B, Patel RV, Whitney J, Deflaux N, Bingham J, Wang Z, Pellecchia G, Buchanan JA, Walker S, Marshall CR, Uddin M, Zarrei M, Deneault E, D'Abate L, Chan AJS, Koyanagi S, Paton T, Pereira SL, Hoang N, Engchuan W, Higginbotham EJ, Ho K, Lamoureux S, Li W, MacDonald JR, Nalpathamkalam T, Sung WWL, Tsoi FJ, Wei J, Xu L, Tasse A-M, Kirby E, Van Etten W, Twigger S, Roberts W, Drmic I, Jilderda S, Modi BM, Kellam B, Szego M, Cytrynbaum C, Weksberg R, Zwaigenbaum L, Woodbury-Smith M, Brian J, Senman L, Iaboni A, Doyle-Thomas K, Thompson A, Chrysler C, Leef J, Savion-Lemieux T, Smith IM, Liu X, Nicolson R, Seifer V, Fedele A, Cook EH, Dager S, Estes A, Gallagher L, Malow BA, Parr JR, Spence SJ, Vorstman J, Frey BJ, Robinson JT, Strug LJ, Fernandez BA, Elsabbagh M, Carter MT, Hallmayer J, Knoppers BM, Anagnostou E, Szatmari P, Ring RH, Glazer D, Pletcher MT, Scherer SW. 2017. Whole genome sequencing resource identifies 18 new candidate genes for autism spectrum disorder. *Nat Neurosci* **20**:602–611. doi:10.1038/nn.4524

Calarco JA, Superina S, O'Hanlon D, Gabut M, Raj B, Pan Q, Skalska U, Clarke L, Gelinas D, van der Kooy D, Zhen M, Ciruna B, Blencowe BJ. 2009. Regulation of vertebrate nervous system alternative splicing and development by an SR-related protein. *Cell* **138**:898–910. doi:10.1016/j.cell.2009.06.012

Capps MES, Moyer AJ, Conklin CL, Martina V, Torija-Olson EG, Klein MC, Gannaway WC, Calhoun CCS, Vivian MD, Thyme SB. 2024. Diencephalic and Neuropeptidergic Dysfunction in Zebrafish with Autism Risk Mutations. *BioRxiv*. doi:10.1101/2024.01.18.576309

Ciampi L, Mantica F, López-Blanch L, Permanyer J, Rodriguez-Marín C, Zang J, Cianferoni D, Jiménez-Delgado S, Bonnal S, Miravet-Verde S, Ruprecht V, Neuhauss SCF, Banfi S, Carrella S, Serrano L, Head SA, Irimia M. 2022. Specialization of the photoreceptor

transcriptome by Srrm3-dependent microexons is required for outer segment maintenance and vision. *Proc Natl Acad Sci USA* **119**:e2117090119. doi:10.1073/pnas.2117090119

Dergai M, Tsyba L, Dergai O, Zlatskii I, Skrypkina I, Kovalenko V, Rynditch A. 2010. Microexon-based regulation of ITSN1 and Src SH3 domains specificity relies on introduction of charged amino acids into the interaction interface. *Biochem Biophys Res Commun* **399**:307–312. doi:10.1016/j.bbrc.2010.07.080

Dreosti E, Lopes G, Kampff AR, Wilson SW. 2015. Development of social behavior in young zebrafish. *Front Neural Circuits* **9**:39. doi:10.3389/fncir.2015.00039

Drerup CM, Nechiporuk AV. 2013. JNK-interacting protein 3 mediates the retrograde transport of activated c-Jun N-terminal kinase and lysosomes. *PLoS Genet* **9**:e1003303. doi:10.1371/journal.pgen.1003303

Emperador-Melero J, Huson V, van Weering J, Bollmann C, Fischer von Mollard G, Toonen RF, Verhage M. 2018. Vti1a/b regulate synaptic vesicle and dense core vesicle secretion via protein sorting at the Golgi. *Nat Commun* **9**:3421. doi:10.1038/s41467-018-05699-z

Giacomini T, Nuovo S, Zanni G, Mancardi MM, Cusmai R, Pepi C, Bertini E, Valente EM, Battini R, Ferrari A, Romaniello R, Zucca C, Borgatti R, Uccella S, Severino M, Striano P, Pistorio A, Prato G, De Grandis E, Nobili L, Pisciotta L. 2021. CASK related disorder: Epilepsy and developmental outcome. *Eur J Paediatr Neurol* **31**:61–69. doi:10.1016/j.ejpn.2021.02.006

Gogou C, Beugelink JW, Frias CP, Kresik L, Jaroszynska N, Drescher U, Janssen BJC, Hindges R, Meijer DH. 2024. Alternative splicing controls teneurin-3 compact dimer formation for neuronal recognition. *Nat Commun* **15**:3648. doi:10.1038/s41467-024-47763-x

Gonatopoulos-Pournatzis T, Blencowe BJ. 2020. Microexons: at the nexus of nervous system development, behaviour and autism spectrum disorder. *Curr Opin Genet Dev* **65**:22–33. doi:10.1016/j.gde.2020.03.007

Gonatopoulos-Pournatzis T, Niibori R, Salter EW, Weatheritt RJ, Tsang B, Farhangmehr S, Liang X, Braunschweig U, Roth J, Zhang S, Henderson T, Sharma E, Quesnel-Vallières M, Permanyer J, Maier S, Georgiou J, Irimia M, Sonenberg N, Forman-Kay JD, Gingras A-C, Collingridge GL, Woodin MA, Cordes SP, Blencowe BJ. 2020. Autism-Misregulated eIF4G Microexons Control Synaptic Translation and Higher Order Cognitive Functions. *Mol Cell* **77**:1176-1192.e16. doi:10.1016/j.molcel.2020.01.006

Gonatopoulos-Pournatzis T, Wu M, Braunschweig U, Roth J, Han H, Best AJ, Raj B, Aregger M, O'Hanlon D, Ellis JD, Calarco JA, Moffat J, Gingras A-C, Blencowe BJ. 2018. Genome-wide CRISPR-Cas9 Interrogation of Splicing Networks Reveals a Mechanism for Recognition of Autism-Misregulated Neuronal Microexons. *Mol Cell* **72**:510-524.e12. doi:10.1016/j.molcel.2018.10.008

Gupta T, Margolin G, Burgess HA. 2025. Mutations in the microexon splicing regulator srrm4 have minor phenotypic effects on zebrafish neural development. *G3 (Bethesda)* **15**. doi:10.1093/g3journal/jkaf052

Han KA, Yoon T-H, Kim J, Lee J, Lee JY, Jang G, Um JW, Kim JK, Ko J. 2024. Specification of neural circuit architecture shaped by context-dependent patterned LAR-RPTP microexons. *Nat Commun* **15**:1624. doi:10.1038/s41467-024-45695-0

Heo J, Larner JM, Brautigan DL. 2020. Protein kinase CK2 phosphorylation of SAPS3 subunit increases PP6 phosphatase activity with Aurora A kinase. *Biochem J* **477**:431–444. doi:10.1042/BCJ20190740

Huang CY-M, Zhang C, Ho TS-Y, Oses-Prieto J, Burlingame AL, Lalonde J, Noebels JL, Leterrier C, Rasband MN. 2017. αii spectrin forms a periodic cytoskeleton at the axon initial segment and is required for nervous system function. *J Neurosci* **37**:11311–11322. doi:10.1523/JNEUROSCI.2112-17.2017

Irimia M, Weatheritt RJ, Ellis JD, Parikshak NN, Gonatopoulos-Pournatzis T, Babor M, Quesnel-Vallières M, Tapial J, Raj B, O'Hanlon D, Barrios-Rodiles M, Sternberg MJE, Cordes SP, Roth FP, Wrana JL, Geschwind DH, Blencowe BJ. 2014. A highly conserved program of neuronal microexons is misregulated in autistic brains. *Cell* **159**:1511–1523. doi:10.1016/j.cell.2014.11.035

Jefferis GSXE, Potter CJ, Chan AM, Marin EC, Rohlfing T, Maurer CR, Luo L. 2007. Comprehensive maps of Drosophila higher olfactory centers: spatially segregated fruit and pheromone representation. *Cell* **128**:1187–1203. doi:10.1016/j.cell.2007.01.040

Joo W, Vivian MD, Graham BJ, Soucy ER, Thyme SB. 2020. A Customizable Low-Cost System for Massively Parallel Zebrafish Behavioral Phenotyping. *Front Behav Neurosci* **14**:606900. doi:10.3389/fnbeh.2020.606900

Kunwar AJ, Rickmann M, Backofen B, Browski SM, Rosenbusch J, Schöning S, Fleischmann T, Krieglstein K, Fischer von Mollard G. 2011. Lack of the endosomal SNAREs vti1a and vti1b led to significant impairments in neuronal development. *Proc Natl Acad Sci USA* **108**:2575–2580. doi:10.1073/pnas.1013891108

Li J, Xie Y, Cornelius S, Jiang X, Sando R, Kordon SP, Pan M, Leon K, Südhof TC, Zhao M, Araç D. 2020. Alternative splicing controls teneurin-latrophilin interaction and synapse specificity by a shape-shifting mechanism. *Nat Commun* **11**:2140. doi:10.1038/s41467-020-16029-7

Lin L, Zhang M, Stoilov P, Chen L, Zheng S. 2020. Developmental Attenuation of Neuronal Apoptosis by Neural-Specific Splicing of Bak1 Microexon. *Neuron* **107**:1180-1196.e8. doi:10.1016/j.neuron.2020.06.036

Lin Z, Liu J, Ding H, Xu F, Liu H. 2018. Structural basis of SALM5-induced PTPδ dimerization for synaptic differentiation. *Nat Commun* **9**:268. doi:10.1038/s41467-017-02414-2

Li Y, Zhang P, Choi T-Y, Park SK, Park H, Lee E-J, Lee D, Roh JD, Mah W, Kim R, Kim Y, Kwon H, Bae YC, Choi S-Y, Craig AM, Kim E. 2015. Splicing-Dependent Trans-synaptic SALM3-LAR-RPTP Interactions Regulate Excitatory Synapse Development and Locomotion. *Cell Rep* **12**:1618–1630. doi:10.1016/j.celrep.2015.08.002

Li YI, Sanchez-Pulido L, Haerty W, Ponting CP. 2015. RBFOX and PTBP1 proteins regulate the alternative splicing of micro-exons in human brain transcripts. *Genome Res* **25**:1–13. doi:10.1101/gr.181990.114

Lopez-Blanch L, Rodríguez-Marin C, Mantica F, Iñiguez LP, Permanyer J, Kita EM, Mackensen T, Codina-Tobias M, Romero-Ferrero F, Fernandez-Albert J, Cuadrado M, Bustelo XR, de Polavieja GG, Irimia M. 2024. Phenotypic impact of individual conserved neuronal microexons and their master regulators in zebrafish. *BioRxiv*. doi:10.1101/2024.10.23.619860

Martinez R, Mathey-Prevot B, Bernards A, Baltimore D. 1987. Neuronal pp60c-src contains a six-amino acid insertion relative to its non-neuronal counterpart. *Science* **237**:411–415. doi:10.1126/science.2440106

Nakano Y, Wiechert S, Bánfi B. 2019. Overlapping Activities of Two Neuronal Splicing Factors Switch the GABA Effect from Excitatory to Inhibitory by Regulating REST. *Cell Rep* **27**:860-871.e8. doi:10.1016/j.celrep.2019.03.072

O'Grady P, Krueger NX, Streuli M, Saito H. 1994. Genomic organization of the human LAR protein tyrosine phosphatase gene and alternative splicing in the extracellular fibronectin type-III domains. *J Biol Chem* **269**:25193–25199. doi:10.1016/S0021-9258(17)31516-8

Parada GE, Munita R, Georgakopoulos-Soares I, Fernandes HJR, Kedlian VR, Metzakopian E, Andres ME, Miska EA, Hemberg M. 2021. MicroExonator enables systematic discovery and quantification of microexons across mouse embryonic development. *Genome Biol* **22**:43. doi:10.1186/s13059-020-02246-2

Park H, Choi Y, Jung H, Kim S, Lee S, Han H, Kweon H, Kang S, Sim WS, Koopmans F, Yang E, Kim H, Smit AB, Bae YC, Kim E. 2020. Splice-dependent trans-synaptic PTPδ-IL1RAPL1 interaction regulates synapse formation and non-REM sleep. *EMBO J* **39**:e104150. doi:10.15252/embj.2019104150

Platzer K, Sticht H, Edwards SL, Allen W, Angione KM, Bonati MT, Brasington C, Cho MT, Demmer LA, Falik-Zaccai T, Gamble CN, Hellenbroich Y, Iascone M, Kok F, Mahida S, Mandel H, Marquardt T, McWalter K, Panis B, Pepler A, Pinz H, Ramos L, Shinde DN, Smith-Hicks C, Stegmann APA, Stöbe P, Stumpel CTRM, Wilson C, Lemke JR, Di Donato N, Miller KG, Jamra R. 2019. De Novo Variants in MAPK8IP3 Cause Intellectual Disability with Variable Brain Anomalies. *Am J Hum Genet* **104**:203–212. doi:10.1016/j.ajhg.2018.12.008

Poliński P, Miret Cuesta M, Zamora-Moratalla A, Mantica F, Cantero-Recasens G, Normanno D, Iñiguez LP, Morenilla-Palao C, Ordoño P, Bonnal S, Ellis JD, Gómez Riera R, De Lagrán Cabredo MM, Fernández-Blanco Á, Rodríguez-Marin C, Permanyer J, Fölsz O, Dominguez-Sala E, Sierra C, Legutko D, Wojnacki J, Musoles Lleo JL, Muñoz López FJ, Blencowe BJ, Herrera E, Dierssen M, Irimia M. 2023. A highly conserved neuronal microexon in DAAM1 controls actin dynamics, RHOA/ROCK signaling, and memory formation. *BioRxiv*. doi:10.1101/2023.01.12.523772

Pulido R, Serra-Pagès C, Tang M, Streuli M. 1995. The LAR/PTP delta/PTP sigma subfamily of transmembrane protein-tyrosine-phosphatases: multiple human LAR, PTP delta, and PTP sigma isoforms are expressed in a tissue-specific manner and associate with the LAR-interacting protein LIP.1. *Proc Natl Acad Sci USA* **92**:11686–11690. doi:10.1073/pnas.92.25.11686

Quesnel-Vallières M, Irimia M, Cordes SP, Blencowe BJ. 2015. Essential roles for the splicing regulator nSR100/SRRM4 during nervous system development. *Genes Dev* **29**:746–759. doi:10.1101/gad.256115.114

Randlett O, Wee CL, Naumann EA, Nnaemeka O, Schoppik D, Fitzgerald JE, Portugues R, Lacoste AMB, Riegler C, Engert F, Schier AF. 2015. Whole-brain activity mapping onto a zebrafish brain atlas. *Nat Methods* **12**:1039–1046. doi:10.1038/nmeth.3581

Rohlfing T, Maurer CR. 2003. Nonrigid image registration in shared-memory multiprocessor environments with application to brains, breasts, and bees. *IEEE Trans Inf Technol Biomed* **7**:16–25. doi:10.1109/titb.2003.808506

Rosenthal SM, Misra T, Abdouni H, Branon TC, Ting AY, Scott IC, Gingras A-C. 2021. A toolbox for efficient proximity-dependent biotinylation in zebrafish embryos. *BioRxiv*. doi:10.1101/2021.05.16.444353

Satyanarayana A, Gudmundsson KO, Chen X, Coppola V, Tessarollo L, Keller JR, Hou SX. 2010. RapGEF2 is essential for embryonic hematopoiesis but dispensable for adult hematopoiesis. *Blood* **116**:2921–2931. doi:10.1182/blood-2010-01-262964

Schindelin J, Arganda-Carreras I, Frise E, Kaynig V, Longair M, Pietzsch T, Preibisch S, Rueden C, Saalfeld S, Schmid B, Tinevez J-Y, White DJ, Hartenstein V, Eliceiri K, Tomancak P, Cardona A. 2012. Fiji: an open-source platform for biological-image analysis. *Nat Methods* **9**:676–682. doi:10.1038/nmeth.2019

Sokpor G, Rosenbusch J, Kunwar AJ, Rickmann M, Tuoc T, Rizzoli SO, Tarabykin V, von Mollard GF, Krieglstein K, Staiger JF. 2021. Ablation of Vti1a/1b Triggers Neural Progenitor Pool Depletion and Cortical Layer 5 Malformation in Late-embryonic Mouse Cortex. *Neuroscience* **463**:303–316. doi:10.1016/j.neuroscience.2021.03.021

Syrbe S, Harms FL, Parrini E, Montomoli M, Mütze U, Helbig KL, Polster T, Albrecht B, Bernbeck U, van Binsbergen E, Biskup S, Burglen L, Denecke J, Heron B, Heyne HO, Hoffmann GF, Hornemann F, Matsushige T, Matsuura R, Kato M, Korenke GC, Kuechler A, Lämmer C, Merkenschlager A, Mignot C, Ruf S, Nakashima M, Saitsu H, Stamberger H, Pisano T, Tohyama J, Weckhuysen S, Werckx W, Wickert J, Mari F, Verbeek NE, Møller RS, Koeleman B, Matsumoto N, Dobyns WB, Battaglia D, Lemke JR, Kutsche K, Guerrini R. 2017. Delineating SPTAN1 associated phenotypes: from isolated epilepsy to encephalopathy with progressive brain atrophy. *Brain* **140**:2322–2336. doi:10.1093/brain/awx195

Thacker S, Sefyi M, Eng C. 2020. Alternative splicing landscape of the neural transcriptome in a cytoplasmic-predominant Pten expression murine model of autism-like Behavior. *Transl Psychiatry* **10**:380. doi:10.1038/s41398-020-01068-x

Thyme SB, Pieper LM, Li EH, Pandey S, Wang Y, Morris NS, Sha C, Choi JW, Herrera KJ, Soucy ER, Zimmerman S, Randlett O, Greenwood J, McCarroll SA, Schier AF. 2019. Phenotypic Landscape of Schizophrenia-Associated Genes Defines Candidates and Their Shared Functions. *Cell* **177**:478-491.e20. doi:10.1016/j.cell.2019.01.048

Torres-Mendez A, Pop S, Bonnal S, Almudi I, Roberts RJV, Paolantoni C, Alcaina A, Avola A, Martin Anduaga A, Haussmann IH, Morin V, Soller M, Kadener S, Roignant J-Y, Prieto-Godino L, Irimia M. 2021. Parallel evolution of a splicing program controlling neuronal excitability in flies and mammals. *BioRxiv*. doi:10.1101/2021.02.24.432780

Tuttle A, Drerup CM, Marra M, McGraw H, Nechiporuk AV. 2019. Retrograde Ret signaling controls sensory pioneer axon outgrowth. *eLife* **8**. doi:10.7554/eLife.46092

Um JW, Kim KH, Park BS, Choi Y, Kim D, Kim CY, Kim SJ, Kim M, Ko JS, Lee S-G, Choii G, Nam J, Heo WD, Kim E, Lee J-O, Ko J, Kim HM. 2014. Structural basis for LAR-RPTP/Slitrk complex-mediated synaptic adhesion. *Nat Commun* **5**:5423. doi:10.1038/ncomms6423

Valente A, Huang K-H, Portugues R, Engert F. 2012. Ontogeny of classical and operant learning behaviors in zebrafish. *Learn Mem* **19**:170–177. doi:10.1101/lm.025668.112

Vuong CK, Black DL, Zheng S. 2016. The neurogenetics of alternative splicing. *Nat Rev Neurosci* **17**:265–281. doi:10.1038/nrn.2016.27

Walter AM, Kurps J, de Wit H, Schöning S, Toft-Bertelsen TL, Lauks J, Ziomkiewicz I, Weiss AN, Schulz A, Fischer von Mollard G, Verhage M, Sørensen JB. 2014. The SNARE protein vti1a functions in dense-core vesicle biogenesis. *EMBO J* **33**:1681–1697. doi:10.15252/embj.201387549

Watt D, Dixit R, Cavalli V. 2015. JIP3 Activates Kinesin-1 Motility to Promote Axon Elongation. *J Biol Chem* **290**:15512–15525. doi:10.1074/jbc.M115.651885

Weinschutz Mendes H, Neelakantan U, Liu Y, Fitzpatrick SE, Chen T, Wu W, Pruitt A, Jin DS, Jamadagni P, Carlson M, Lacadie CM, Enriquez KD, Li N, Zhao D, Ijaz S, Sakai C, Szi C, Rooney B, Ghosh M, Nwabudike I, Gorodezky A, Chowdhury S, Zaheer M, McLaughlin S,

Fernandez JM, Wu J, Eilbott JA, Vander Wyk B, Rihel J, Papademetris X, Wang Z, Hoffman EJ. 2023. High-throughput functional analysis of autism genes in zebrafish identifies convergence in dopaminergic and neuroimmune pathways. *Cell Rep* **42**:112243. doi:10.1016/j.celrep.2023.112243

Wu G, Li D, Liang W, Sun W, Xie X, Tong Y, Shan B, Zhang M, Lu X, Yuan J, Li Y. 2022. PP6 negatively modulates LUBAC-mediated M1-ubiquitination of RIPK1 and c-FLIPL to promote TNFα-mediated cell death. *Cell Death Dis* **13**:773. doi:10.1038/s41419-022-05206-9

Yamagata A, Sato Y, Goto-Ito S, Uemura T, Maeda A, Shiroshima T, Yoshida T, Fukai S. 2015. Structure of Slitrk2-PTPδ complex reveals mechanisms for splicing-dependent trans-synaptic adhesion. *Sci Rep* **5**:9686. doi:10.1038/srep09686

Yim YS, Kwon Y, Nam J, Yoon HI, Lee K, Kim DG, Kim E, Kim CH, Ko J. 2013. Slitrks control excitatory and inhibitory synapse formation with LAR receptor protein tyrosine phosphatases. *Proc Natl Acad Sci USA* **110**:4057–4062. doi:10.1073/pnas.1209881110

Figure Legends

Fig. 1. Generation and analysis of zebrafish with mutations that remove conserved, developmentally regulated microexons. (**A**) Pipeline of the screen. Mutant lines with alternatively spliced microexons removed were generated with CRISPR/Cas9, crossed together, and sibling larvae were assessed for changes to brain morphology, brain activity, and behavioral profiling. Created with BioRender.com. (**B**) The amino acid sequence identity of 95 zebrafish microexons compared to mouse. (**C**) The amino acid sequence identity of 95 zebrafish microexons compared to mouse and divided by the sequence identity of the entire protein. (**D**) Gene Ontology analysis of biological processes associated with the 95 mouse microexons that are conserved in zebrafish. The analysis was completed using the PANTHER classification system. (**E**) Quantification of reverse transcription PCR (RT-PCR) for microexon-containing regions over zebrafish development. These data were clustered using the default seaborn clustermap settings (method = 'average').

Fig. 2. Larval behavioral phenotypes of zebrafish with microexons removed. (**A**) Summary of behavioral pipeline. (**B**) Baseline behavioral phenotypes for microexon mutants. The labels "1" and "2" indicate biological replicates. The data shown is for homozygous mutant larvae compared to wild-type siblings. Comparisons to the heterozygous larvae are removed for clarity and available in the Supplementary Materials, as they often have even milder phenotypes than homozygous. The size of the bubble represents the percent of significant measurements in the summarized category, and the color represents the mean of the strictly standardized mean difference (SSMD) of the significant assays in that category. (**C**) Stimulus-driven behavioral phenotypes for microexon mutants. The labels "1" and "2" indicate biological replicates. The bubble size and color are calculated the same as in panel B. (**D**) Examples of behavioral phenotypes. The black boxes in panels B and C correspond to the selected plots. Wild-type siblings (black) are compared to the homozygous (red), and the plots show mean ± s.e.m.. All N are in Table S2. Kruskal-Wallis ANOVA p-values for the selected plots are as follows: *dop1a* center preference during the first night (day0night_boutcenterfraction_3600) = 0.00006/0.0008, N +/+ = 15 (run 1) and 14 (run 2), N -/- = 17 (run 1) and 15 (run 2); *eif4g3b* p-values are not calculated for response traces (shown is all dark flashes in block 1), p-values for the latency for the first 10 dark flashes in block 1 (day6dpfdf1a_responselatency) = 0.026/0.0008, N +/+ = 16 (run 1) and 15 (run 2), N -/- = 15 (run 1) and 21 (run 2); *ppp6r3* frequency of response to strong acoustic stimuli with a sound frequency of 1000 hertz that precede the habituation block (day5dpfhab1pre_responsefrequency_1_a1f1000d5p) = 0.002/0.016, N +/+ = 19 (run 1) and 20 (run 2), N -/- = 21 (run 1) and 29 (run 2); *ptprd*-1 pixels moved in each bout for the duration of the experiment (combo_boutcumulativemovement_3600) = 0.001/0.00002, N +/+ = 22 (run 1) and 21 (run 2), N -/- = 26 (run 1) and 18 (run 2); *rapgef2* number of bouts for the duration of the experiment calculated using the delta pixel data in each frame (dpix_numberofbouts_3600) = 0.002/0.001, N +/+ = 21 (run 1) and 23 (run 2), N -/- = 21 (run 1) and 20 (run 2).

Fig. 3. Whole-brain activity and morphology phenotypes of zebrafish with microexons removed. (**A**) Clustered summary of pErk comparisons between homozygous mutants and wild-type control siblings, where magenta represents decreased activity and green represents increased. The signal in each region was summed and divided by the region size. The N for all experiments is available in Table S2. (**B**) Clustered summary of structure comparisons between

homozygous mutants and wild-type control siblings, where magenta represents decreased size and green represents increased. (**C**) Location of major regions in the zebrafish brain based on masks from the Z-Brain atlas (Randlett et al., 2015). (**D**) Brain imaging for microexon mutants with repeatable brain activity phenotypes. The brain images represent the significant signal difference between homozygous and wild-type control siblings. They are shown as sum-of-slices projections (Z- and X- axes) with the white outline representing the zebrafish brain. (**E**) Structural phenotype of the *ppp6r3* mutant, with replicates shown side-by-side. The magenta indicates decreased size. (**F**) Brain imaging for two microexon mutants with brain activity phenotypes that are similar for both the heterozygous and homozygous mutants. (**G**) Comparison of the total brain activity signal between homozygous microexon mutants from this work and mutants for autism risk genes from (Capps et al., 2024). Both increased and decreased activity are considered and a single comparison rather than the average of the repeats.

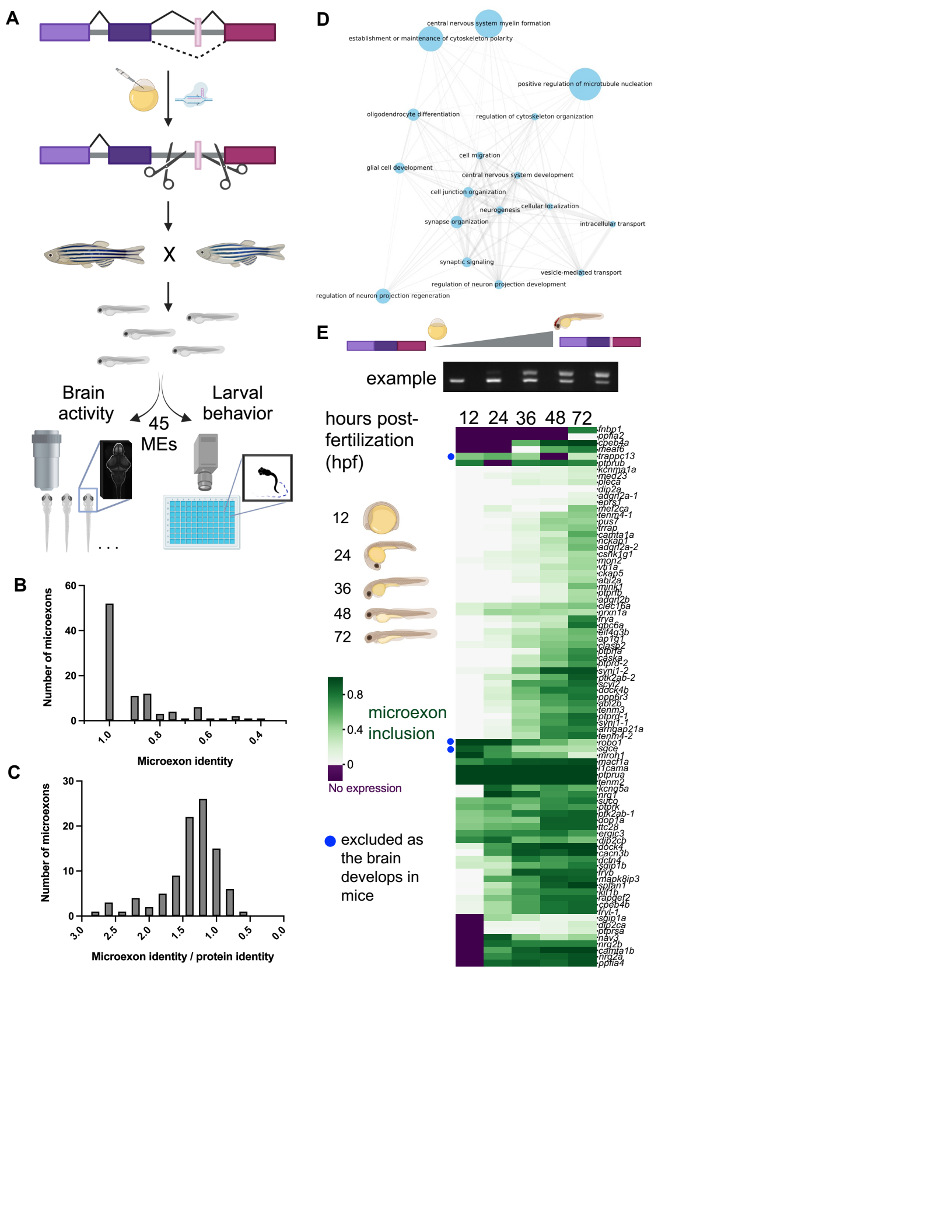
A
X
Brain activity
45 MEs
Larval behavior
B
Number of microexons
Microexon identity
C
Number of microexons
Microexon identity / protein identity
D
central nervous system myelin formation
establishment or maintenance of cytoskeleton polarity
positive regulation of microtubule nucleation
oligodendrocyte differentiation
regulation of cytoskeleton organization
cell migration
glial cell development
central nervous system development
cell junction organization
neurogenesis
cellular localization
synapse organization
intracellular transport
synaptic signaling
vesicle-mediated transport
regulation of neuron projection development
regulation of neuron projection regeneration
E
example
hours post-fertilization (hpf)
12 24 36 48 72
microexon inclusion
No expression
excluded as the brain develops in mice

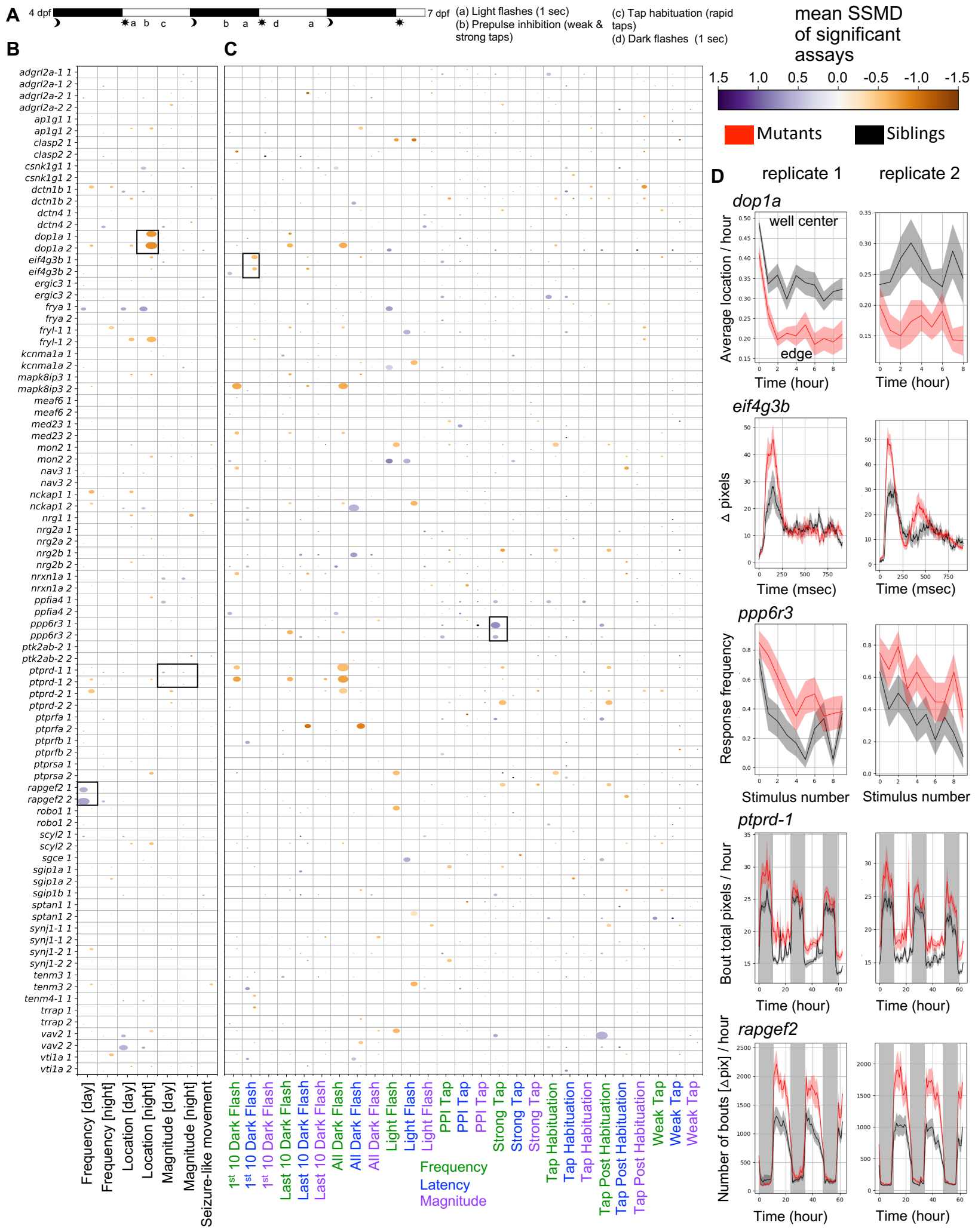
A
4 dpf
7 dpf
a b c
b a d a
(a) Light flashes (1 sec)
(b) Prepulse inhibition (weak & strong taps)
(c) Tap habituation (rapid taps)
(d) Dark flashes (1 sec)
mean SSMD of significant assays
1.5 1.0 0.5 0.0 -0.5 -1.0 -1.5
Mutants
Siblings
B
C
Frequency [day]
Frequency [night]
Location [day]
Location [night]
Magnitude [day]
Magnitude [night]
Seizure-like movement
1st 10 Dark Flash
Last 10 Dark Flash
All Dark Flash
Light Flash
PPI Tap
Strong Tap
Tap Habituation
Tap Post Habituation
Weak Tap
Frequency
Latency
Magnitude
D
replicate 1
replicate 2
dop1a
well center
edge
Average location / hour
Time (hour)
eif4g3b
Δ pixels
Time (msec)
ppp6r3
Response frequency
Stimulus number
ptprd-1
Bout total pixels / hour
Time (hour)
rapgef2
Number of bouts [Δpix] / hour
Time (hour)

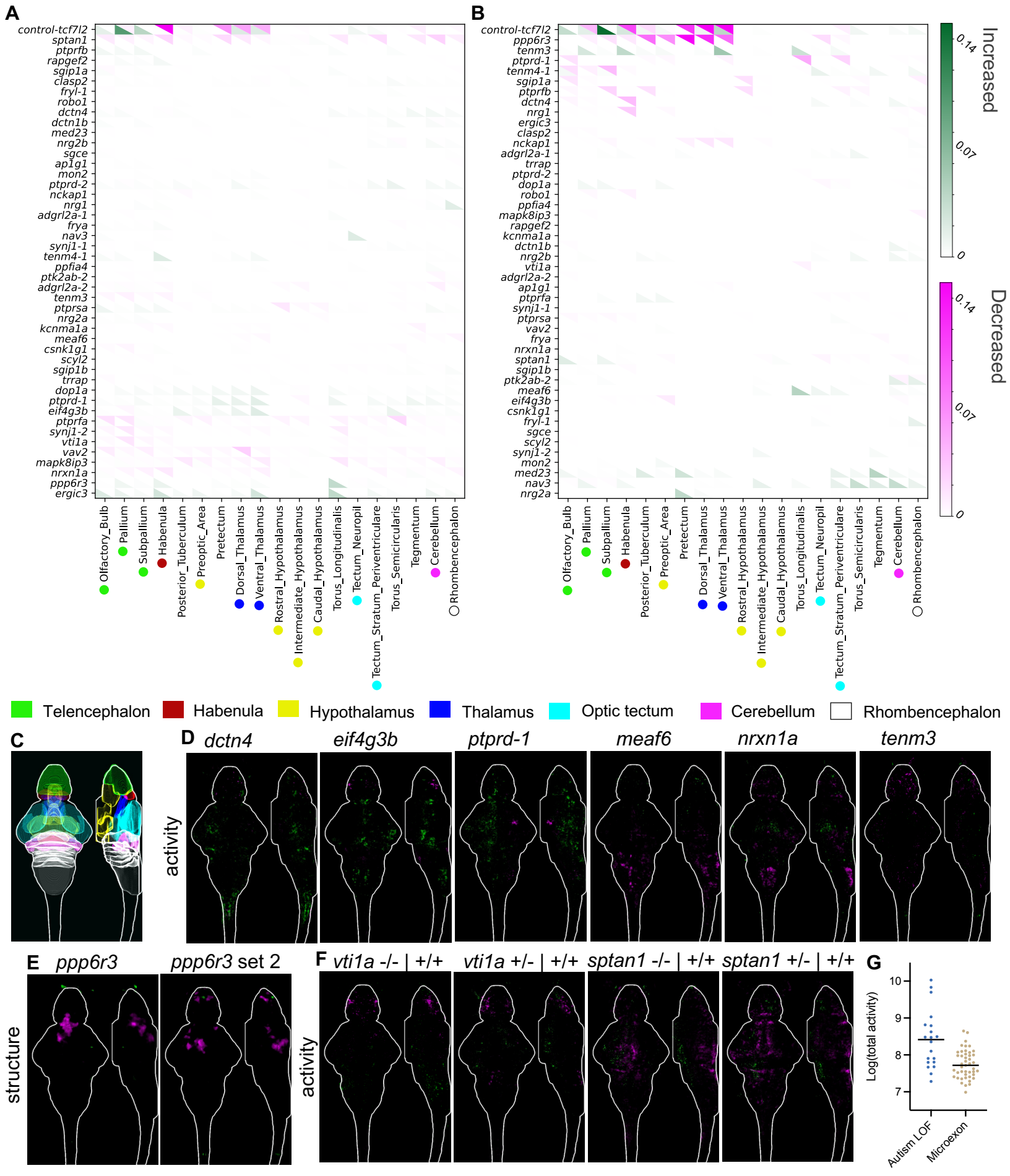
A
B
control-tcf7l2
sptan1
ptprfb
rapgef2
sgip1a
clasp2
fryl-1
robo1
dctn4
dctn1b
med23
nrg2b
sgce
ap1g1
mon2
ptprd-2
nckap1
nrg1
adgrl2a-1
frya
nav3
synj1-1
tenm4-1
ppfia4
ptk2ab-2
adgrl2a-2
tenm3
ptprsa
nrg2a
kcnma1a
meaf6
csnk1g1
scyl2
sgip1b
trrap
dop1a
ptprd-1
eif4g3b
ptprfa
synj1-2
vti1a
vav2
mapk8ip3
nrxn1a
ppp6r3
ergic3
ppp6r3
tenm3
ptprd-1
tenm4-1
sgip1a
ptprfb
dctn4
nrg1
ergic3
clasp2
nckap1
adgrl2a-1
trrap
ptprd-2
dop1a
robo1
ppfia4
mapk8ip3
rapgef2
kcnma1a
dctn1b
nrg2b
vti1a
adgrl2a-2
ap1g1
ptprfa
synj1-1
ptprsa
vav2
frya
nrxn1a
sptan1
sgip1b
ptk2ab-2
meaf6
eif4g3b
csnk1g1
fryl-1
sgce
scyl2
synj1-2
mon2
med23
nav3
nrg2a
Olfactory_Bulb
Pallium
Subpallium
Habenula
Posterior_Tuberculum
Preoptic_Area
Pretectum
Dorsal_Thalamus
Ventral_Thalamus
Rostral_Hypothalamus
Intermediate_Hypothalamus
Caudal_Hypothalamus
Torus_Longitudinalis
Tectum_Neuropil
Tectum_Stratum_Periventriculare
Torus_Semicircularis
Tegmentum
Cerebellum
Rhombencephalon
Increased
Decreased
0.14
0.07
0
Telencephalon
Habenula
Hypothalamus
Thalamus
Optic tectum
Cerebellum
Rhombencephalon
C
D
dctn4
eif4g3b
ptprd-1
meaf6
nrxn1a
tenm3
activity
E
ppp6r3
ppp6r3 set 2
structure
F
vti1a -/- | +/+
vti1a +/- | +/+
sptan1 -/- | +/+
sptan1 +/- | +/+
activity
G
Log(total activity)
10
9
8
7
Autism LOF
Microexon